Mon. Not. R. Astron. Soc. **000**, 000–000 (1994) Printed 1 February 2008 (MN plain TEX macros v1.6)

# The environments of intermediate-redshift QSOs: $0{\cdot}3 < z < 0{\cdot}7$

R. J. Smith[1,2], B. J. Boyle[3] and S. J. Maddox[1,4]

[1] *Institute of Astronomy, University of Cambridge, Madingley Road, Cambridge, CB3 0HA, UK*
[2] *Research School of Astronomy and Astrophysics - Mount Stromlo Observatory, Institute of Advanced Studies, Australian National University, Private bag, Weston Creek P.O., ACT 2611, Australia*
[3] *Anglo-Australian Observatory, PO Box 296, Epping, NSW 2121, Australia*
[4] *School of Physics & Astronomy, University of Nottingham, University Park, Nottingham NG7 2RD, UK*



**ABSTRACT**

An angular correlation of low significance ($2\sigma$) is observed between $0{\cdot}3 < z < 0{\cdot}5$ QSOs and $V \leq 23$ galaxies. Overall, the cross-correlation function between 82 intermediate-redshift ($0{\cdot}3 < z < 0{\cdot}7$), X-ray selected QSOs and $V \lesssim 24$ galaxies is investigated, but no signal is detected for the $z > 0{\cdot}5$ QSOs. After converting to an excess of galaxies physically associated with the QSO, this lack of strong correlation is shown to be consistent with the clustering of normal galaxies at the same moderate redshifts. Combined with previous observations, these results imply that the environments of radio-quiet QSOs do not undergo significant evolution with respect to the galaxy population over a wide range of redshifts ($0 < z < 1{\cdot}5$). This is in marked contrast to the rapid increase in the richness of the environments associated with radio-loud QSOs over the same redshift range.

**Key words:** Quasars: general – galaxies: clusters: general – galaxies: active

## 1 INTRODUCTION

The study of QSO environments provides a direct measure of the bias in their distribution with respect to galaxies. This not only provides insights into the triggering/fuelling mechanism of QSOs, but assists in the relating the results from QSO clustering studies (see e.g., Croom & Shanks 1996, La Franca, Andreani & Cristiani 1998) to large-scale structure studies carried out with galaxy redshift surveys.

We have already investigated the galaxy cluster environments of low-redshift QSOs (Smith, Boyle & Maddox 1995, hereinafter Paper I). The results of this study demonstrated that radio-quiet QSOs exist in average galaxy environments, consistent with these QSOs and galaxies having the same clustering amplitude. However, the observed objects were all at low redshift ($z \leq 0{\cdot}3$), and at low luminosity ($M_B > -24$). In this paper we extend this work to higher redshifts and higher luminosities, probing the region of $M_B, z$ space where the forthcoming large QSO surveys (2dF, Sloan) are targetted.

Previous surveys have been limited by relatively small samples of radio-quiet objects, particularly in the redshift range $0{\cdot}3 < z < 0{\cdot}7$. Yee and collaborators (Yee & Green 1984, 1987, Ellingson, Yee & Green 1991) have previously studied the environments of predominantly radio-loud QSOs at $z < 0{\cdot}6$ and noted significant evolution in the environments of QSOs towards rich clusters at higher redshift. For radio-quiet QSOs Ellingson et al. (1991) measure an amplitude of $1{\cdot}1 \pm 0{\cdot}6$ times the mean, zero-redshift galaxy autocorrelation amplitude and see no evidence for evolution over the redshift range, $0{\cdot}25 < z < 0{\cdot}6$. At higher redshifts ($1 < z < 1{\cdot}5$), most studies (Boyle & Couch 1993, Croom & Shanks 1998) find no significant clustering around radio-quiet QSOs.

In comparison to earlier studies, the advantages of the present work are in the increased number of fields observed and the homogeneous, X-ray selection of QSOs. We are also assisted by having larger and fainter galaxy redshift surveys available with which to compare our results.

In Section 2 we describe the data and its reduction. Section 3 summarises the techniques for measurement of the angular clustering amplitude and the estimation from this of a spatial clustering amplitude. Section 4 describes and discusses the results and a summary is presented in Section 5.

Except where explicitly stated to the contrary, an Einstein–de Sitter Universe has been assumed throughout. That is, $\Omega_0 = 1$, $q_0 = 0{\cdot}5$ and $\Lambda_0 = 0$. The Hubble constant is taken as $100h\,\mathrm{km\,s^{-1}\,Mpc^{-1}}$.

## 2 DATA REDUCTION

### 2.1 Observations

We used deep $V$-band CCD images to detect faint ($V < 24$) galaxies around QSOs in the redshift range $0{\cdot}3 < z < 0{\cdot}7$. QSOs were drawn from the EMSS (Stocke et al. 1991) and CRSS (Boyle et al. 1997) serendipity surveys which use *Einstein* and *ROSAT* data respectively. Details of the EMSS data and the significance of X-ray selection are covered in Paper I. Here we simply note that X-ray selection ensures a fair sample of the general QSO population (Avni & Tananbaum 1986). It is largely insensitive to bias in radio luminosity and spectral index (Zamorani et al. 1981, Della Ceca et al. 1994) and to moderate amounts of dust extinction

(Boyle & Di Matteo 1995) that can in principle seriously affect optical selection techniques.

$V$-band CCD images were obtained of 10-arcminute fields around 82 X-ray selected AGNs in the redshift range, $0{\cdot}3 < z < 0{\cdot}7$ during two observing runs (17–23/09/95 & 15–21/04/96) at the 2·5-metre Isaac Newton Telescope (INT) on La Palma. The same 1024×1024 thinned *Tek3* CCD camera was used on both occasions. The *Tek3* chip has a peak quantum efficiency of 75 per cent at 6500Å (>60 per cent throughout 4000–7700Å) and mounted at the prime focus of the INT, a pixel scale of 0·5896 arcsec pixel$^{-1}$. The field-of-view corresponds to $2{\cdot}1\,h^{-1}$Mpc at $z = 0{\cdot}5$. The CCD was read out in 'Quick' mode; read noise 5·9 electrons, gain 1·44 electrons ADU$^{-1}$. Exposures varied from 15 minutes to 1 hour depending on the QSO's redshift and seeing conditions at the time. In total 69 EMSS and 13 CRSS QSOs were observed. The redshift and absolute magnitude distributions of the sample are shown in Fig. 1.

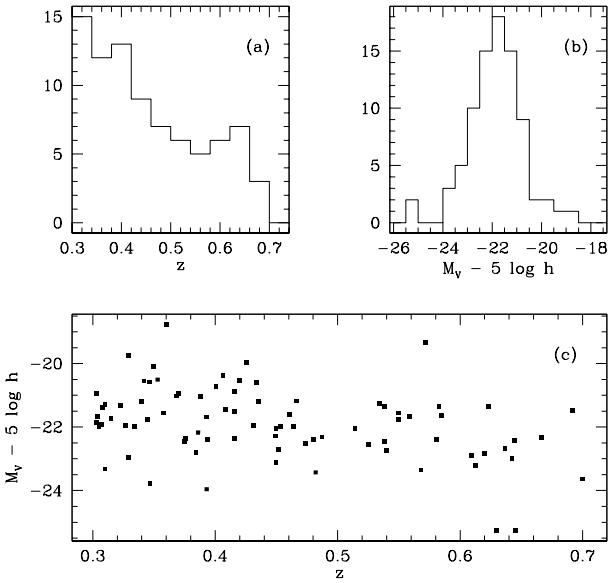


**Figure 1.** (a) Redshift histogram of the 82 QSOs in the sample. (b) Absolute magnitude histogram. (c) Redshift and absolute magnitude are weakly correlated, a natural consequence of both evolution in the QSO luminosity function and this being a flux-limited sample.

### 2.2 Source detection

Raw images were bias subtracted, flat-fielded and coadded using the `imred.ccdred` package in `IRAF`. Source detection, extraction, classification and photometry were carried out using the `SExtractor` software (Bertin & Arnouts 1996). Each image was convolved with a Gaussian filter with full width at half maximum (fwhm) equal to the image's seeing, a background map determined and potential sources selected as connected groups of at least five pixels, each of which were individually greater than $1\sigma$ above the background. For more details of the detection and extraction process, see Bertin & Arnouts (1996).

Most fields contained saturated stars, artificial satellite trails and other defects. Such objects make detection of faint galaxies in their immediate vicinity difficult, so these regions were excised from the survey area in a semi-automated manner (see Smith 1998 for details). As an illustration, the holes used for field MS01084+383, a very low Galactic latitude ($b = -24°$) field significantly affected by bright stars, are shown in Fig. 2a.

To optimise source detection and classification, it is necessary to know the seeing a priori. This information is used to choose a convolution filter for each frame and as the single input parameter into the star–galaxy separation algorithm (see below and Bertin & Arnouts 1996). The `SExtractor` software was therefore run on each frame twice. After the first run, the output catalogue contains the fwhm of every object in the frame allowing an accurate assessment of the seeing, which was taken as the modal fwhm value for unsaturated images. See Fig 2b. These seeing estimates were inspected individually. In a few cases with poor seeing the modal fwhm was not a robust estimate because of a broad scatter in the stellar locus. For these the seeing was estimated by inspection of the data frame and measuring individual clearly stellar objects. In following this procedure it was consistently shown that more objects were detected in the second pass and the star–galaxy separation was more reliable. It was also confirmed that the second pass did not alter the assessment of the seeing.

### 2.3 Photometric calibration

Weather conditions during the observing runs did not merit calibration by photometric standard stars, so the CCD images were calibrated by comparison with previously published, photometrically calibrated deep number–magnitude counts. We used the deep $V$-band galaxy counts of Smail et al. (1995) and we took the stellar counts from the Galaxy model of Bahcall & Soneira (1980).

By fitting the instrumental magnitude number counts from the CCD data to the star-plus-galaxy counts expected on the basis of the chosen models, the only free parameter was the photometric zero-point. The best fit was defined as that giving the minimum absolute deviation between the published and instrumental counts between $V = 20$ and 0·5 magnitude brighter than the peak in the instrumental counts. The observed number counts were generally found to maintain an excellent fit to the model counts at $V < 20$ until the CCD saturated at $V \approx 18$. The full catalogue was used in order to prevent errors in the star–galaxy separation from propagating into the calibration. One such calibration plot is shown in Fig. 2d. The observed number counts are shown as a histogram. The expected counts are shown as the solid curve, with the stellar and galaxian counts plotted individually as dotted curves. Note that this is a low Galactic latitude ($b = -24°$) field and the inclusion of the stellar counts becomes very important. For high Galactic latitude fields, the Smail et al. galaxy counts alone provide an adequate fit to the shape of the observed counts.

This method of calibration is subject to intrinsic variations in the source number density, which are small at faint limits, and to the Poisson error on the counts. Assuming the $b_J \leq 24$ galaxy auto-correlation of Roche et al. (1993) and

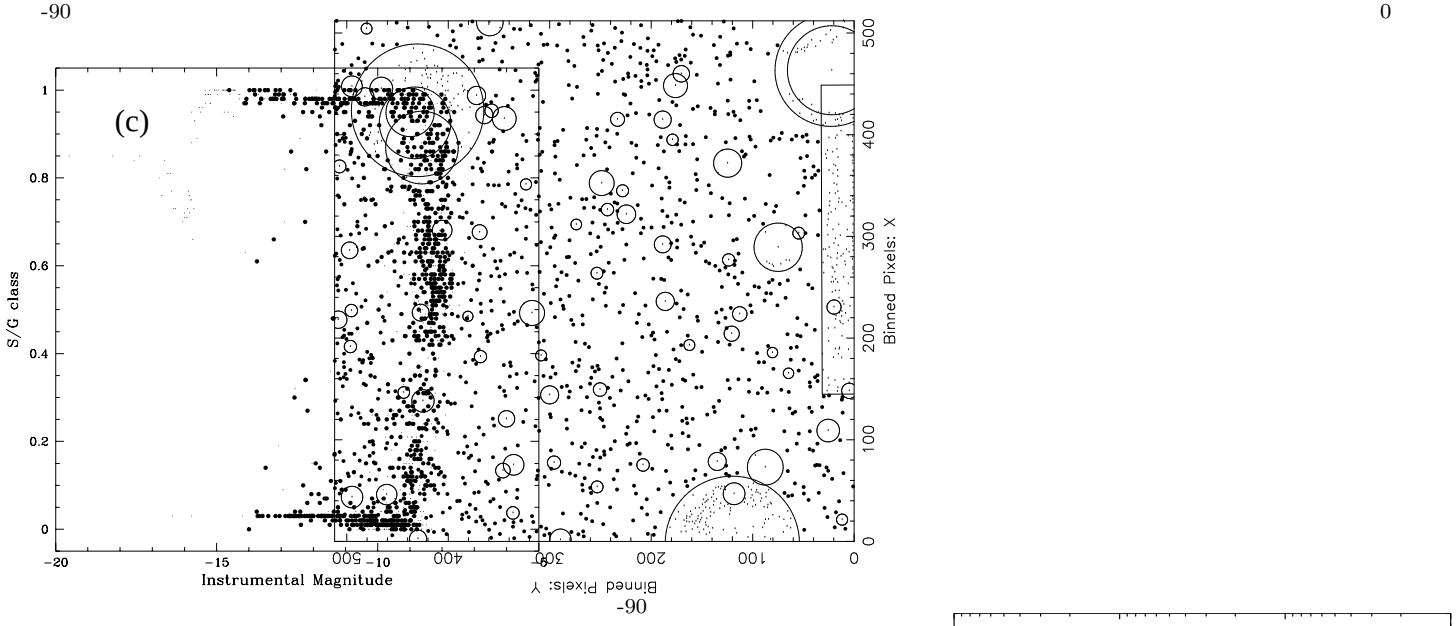


**Figure 2.** Four plots showing aspects of the reduction and photometric calibration process for one particular field, MS01084+383. From the top left: (a) All the sources detected in the field. The 1024 × 1024 pixel *Tek* CCD has been re-binned to 512 × 512 pixels for display purposes only. Large circles and squares show regions of the frame excised for any reason, usually proximity to a saturated star. (b) Determination of the seeing parameter. The horizontal line shows the selected value for the stellar fwhm in pixels. (c) A scatter plot of the star–galaxy classification flag against instrumental magnitude. A value of unity signifies a star and zero a galaxy. Values between these extremes lie on a non-linear probability function of being stellar. In all three plots, large points show sources included in the final catalogue while small dots are objects which fall in regions of the frame excised for any reason. Note that saturated stars deviate significantly from a point-source profile (panel b) and are successfully rejected (appear as small dots) rather than mis-classified as galaxies (panel c). The final panel (d) shows determination of the photometric zero-point. The solid curve is the expected number counts and the histogram the observed counts. Calibration consists of sliding the histogram horizontally until the best fitting position is found. The dotted lines are the expected counts for stars and galaxies plotted separately.

integrating over the CCD field of view, intrinsic galaxy clustering introduces an error of less than 0·01 mag. The star counts model is only claimed to have a 15 per cent accuracy, but since stars typically constitute much less than five per cent of the sources, they also only introduce an error of order 0·01 mag. In the very low Galactic latitude fields, it may be as much as 0·03 mag. With at least five hundred sources used in the calibration for each field, the Poisson error introduces an uncertainty of less than 0·05 mag.

### 2.4 Star–galaxy separation

The fields investigated cover a wide range of Galactic latitudes. Whilst the majority have latitudes $|b| \geq 40°$, there are a significant number nearer the Galactic plane and eight fields were observed at as low as $|b| < 30°$. Stellar contamination of the galaxy catalogue will reduce the amplitude of any observed correlation (see Section 3.3). At low Galactic latitudes in particular, removal of the stars is therefore im-

portant. This may be done by excising the stars from the catalogue before estimating the correlation function, or by estimating the amount of contamination and re-scaling the correlation function to account for it. Both approaches were followed producing results entirely consistent within the statistical errors. The results quoted herein are based on the procedure that used the star–galaxy classification.

The classification as stars or galaxies was achieved using the algorithm in the `SExtractor` package, which produces a classification flag with a value lying between 0 (extended) and 1 (compact). A value of 0·8 was chosen as the boundary between stellar and galaxian images by inspection of plots such as Fig. 2c. This value includes the full width of the locus of points at $\sim 1$ while excluding the cluster which frequently appears at $\sim 0{\cdot}5$. Such a cluster is seen only weakly in the example shown here, but is much more pronounced for some fields. The algorithm's defaulting to values $\sim 0{\cdot}5$ is effectively a *don't-know* classification, but our cut of 0·8 means such objects are called galaxies.

Checks of the validity of the star–galaxy separation process, including the generation of artificial data using the `artdata` package in `IRAF` demonstrated that the star–galaxy classification procedure gave reliable results (see Smith 1998).

### 2.5 The minimum observable angular scale

Artificial data generated by the `artdata` package was also used to establish the effect of the bright QSO on detection of nearby faint galaxies. In order to do this 10 000 small ($100 \times 100$ pixels) simulations were carried out using input parameters selected randomly from distributions defined by the complete CCD data set. The seeing, zero point, QSO magnitude and background level were all varied in this way (see Smith 1998 for details). Each image was furnished with sources down to one magnitude fainter than the CCD completeness and then extracted and identified as usual. There was a marked failure to find galaxies within a few pixels of the modelled QSO. The ratio between the number of simulated and detected sources was computed as a function of radius from the QSO. At distances greater than sixteen pixels, the bright saturated object no longer had a detrimental effect and the source detection success rate was constant, but it decreased rapidly nearer the QSO. At less than five pixels from the QSO, the source detection rate was virtually zero. No counts were therefore performed closer than 5 pixels to the QSO. A best fitting, smooth polynomial was determined to give a correction factor for counts at separations between 5 and 16 pixels. Though locally very significant, the 5 to 16 pixel annulus is very small, so its overall impact on observed counts is also small and makes only a quantitative, not qualitative difference to the results. For example, counts out to one arcminute required multiplication by 1·0053 to compensate for the erroneously low counts in the central few arcseconds.

## 3 ANALYSIS

### 3.1 The correlation function

The QSO–galaxy angular correlation function, $w_{qg}(\theta)$, measures the statistical excess of galaxies observed near the QSO over that expected for a random distribution of the same number of galaxies. In its standard form it may be defined

$$n(\theta)\delta\Omega = N_g[1 + w_{qg}(\theta)]\delta\Omega, \tag{1}$$

where $n(\theta)\delta\Omega$ is the number of galaxies observed in solid angle $\delta\Omega$ at angular separation $\theta$ from the QSO. $N_g$ is the background surface density of galaxies. The galaxy auto-correlation function may be defined similarly as the joint probability of finding a galaxy in both solid angle elements $\delta\Omega_1$ and $\delta\Omega_2$ separated by angle $\theta$.

$$\delta P(\theta) = N_g[1 + w_{gg}(\theta)]\delta\Omega_1\delta\Omega_2 \tag{2}$$

The galaxy angular correlation function has been extensively studied (e.g., Groth & Peebles 1977, Maddox et al. 1990) and found to be well fit at scales less than $5^\circ$ by a power-law of the form

$$w_{gg}(\theta) = A_{gg}\theta^{1-\gamma}, \tag{3}$$

where $A_{gg}$ is the angular covariance amplitude. The power-law slope is measured to be in the range $1{\cdot}7 < \gamma < 1{\cdot}8$. We here assume the QSO–galaxy correlation function to be of the same form,

$$w_{qg}(\theta) = A_{qg}\theta^{1-\gamma} \tag{4}$$

We define $A_{qg}$ to be the amplitude at one degree except where explicitly stated to the contrary.

Measurement of the angular covariance amplitude alone does not tell us about the physical environment of the QSO. We are integrating along the line of sight to the QSO, including information about the foreground and background galaxy populations. The more physically relevant spatial covariance amplitude, $B_{qg}$, gives the strength of spatial clustering of galaxies actually associated with the QSO. The approach adopted here is to compare this with the galaxies' own clustering amplitude, $B_{gg}$, to determine the relative environmental properties of QSOs and galaxies.

By analogy to equation 1, the spatial cross-correlation function, $\xi_{qg}(r)$, is defined as

$$n(r)\delta V = \rho_g[1 + \xi_{qg}(r)]\delta V, \tag{5}$$

where $n(r)\delta V$ are the counts in volume $\delta V$ at distance $r$ from the QSO and $\rho_g$ is the average volume density of galaxies. The galaxy auto-correlation function is similarly defined as

$$\delta P(\theta) = \rho_g^2[1 + \xi_{gg}(r)]\delta V_1\delta V_2 \tag{6}$$

Limber's Equation (Limber 1953) relates the amplitudes of the angular and spatial auto-correlations and shows that equation 3 is a natural consequence of spatial clustering of the form

$$\xi_{gg}(r) = B_{gg}r^{-\gamma} = \left(\frac{r}{r_{0,gg}}\right)^{-\gamma}. \tag{7}$$

Measurements are quoted in the literature either as the spatial covariance amplitude $B_{gg}$, or as a correlation length $r_{0,gg}$. QSO–galaxy cross-correlations have not been measured to sufficient precision to allow a free fit, but are generally assumed to follow the same simple power-law form. (e.g., Yee & Green 1987).

$$\xi_{qg}(r) = B_{qg}r^{-\gamma} = \left(\frac{r}{r_{0,qg}}\right)^{-\gamma}. \tag{8}$$

Longair & Seldner (1979), hereinafter LS79, showed how to convert an observed $A_{qg}$ to an implied $B_{qg}$. A similar approach is adopted here with minor modifications. The conversion is performed in a statistical sense, since the galaxy redshifts are not available. We therefore make several well-justified assumptions relating to the redshift distribution of galaxies and the form and evolution of the galaxy clustering.

First, all clusters are taken to be spherically symmetric. This may not be so for individual cases, but is reasonable when averaged over a large sample. Secondly, we need to allow for the redshift distribution of galaxies, though not the actual redshift of any particular object. Previous applications of this technique have predominantly derived an $N(z)$ from a fixed luminosity function (LS79, Yates, Miller & Peacock 1989, Boyle & Couch 1993). Though it is possible to improve on this by using an evolving luminosity function (Ellis et al. 1996, Maddox et al. 1990), we have here adopted the parametric fit to observational redshift-survey data by Efstathiou (1995). (See also Baugh & Efstathiou 1993, Maddox, Efstathiou & Sutherland 1996.) Deep redshift surveys (e.g., Glazebrook et al. 1995) and studies of weak lensing around rich galaxy clusters (Smail, Ellis & Fitchett 1994) mean the $N(z)$ relation for $B < 24$ galaxies is now well determined, and this offers a more directly observational route to obtaining the required data. The parametric form for the galaxy number-redshift relation derived by Efstathiou (1995) is given by,

$$\frac{\mathrm{d}N}{\mathrm{d}z} \propto z^2 \exp\left\{-\left[\frac{z}{z_c(b_J)}\right]^{3/2}\right\} \tag{9a}$$

$$z_c(b_J) = \begin{cases} 0{\cdot}0113(b_J-17)^{1{\cdot}5} + 0{\cdot}0325 & 17 \le b_J \le 22 \\ 0{\cdot}0010(b_J-17)^3 + 0{\cdot}0325 & b_J > 22 \end{cases} \tag{9b}$$

The relation was normalised assuming a mean galaxy $b_J - V = 0{\cdot}5$, from the same Smail et al. (1995) $V$-band counts as used for the photometric calibration in Section 2.3. The mean galaxy $B - V$ colour was derived from the data of Fukugita, Shimasaku & Ichikawa (1995) and Driver et al. (1994), using the morphology mix shown in Table 1 (see Prestage & Peacock 1988), and converted to $b_J - V$ via the colour equations of Blair & Gilmore (1982). The redshift distributions used are shown in Fig. 3.

Finally LS79 assumed that the clustering is stable in proper coordinates. This is the case for virialized clusters where the structures behave as particles within the expanding Universe. On larger scales or for younger, non-virialized clusters, there is an intrinsic expansion or contraction within the cluster superimposed on the Hubble expansion. For a cluster simply expanding with the Hubble flow, the clustering signal is constant in comoving coordinates. This is expected in the case of sources that have a constant high bias, where the distribution of sources is determined by the initial conditions, largely independent of dynamical evolution.

The rate of clustering evolution is here included as a free parameter, which makes the following changes to the derivation in LS79. Following Phillipps et al. (1978), we assume that only the amplitude varies with redshift, the form remaining constant. Equation 8 becomes,

$$\xi_{qg}(r,z) = B_{0,qg} f(z) r^{-\gamma}. \tag{10}$$

Let the typical cluster scale length, $R$, evolve as $R(z) \propto (1+z)^{-\beta}$. From the definition of the correlation function (equation 1), the excess number of galaxies, $N_e$, in a shell around the QSO is

$$N_e = \rho_g(z)\delta V(z)\xi_{qg}(R(z),z). \tag{11}$$

This shell is then scaled with redshift according to the proposed evolution model. For observations to progressively higher redshifts, the volume sampled changes, making $\rho_g(z) \propto (1+z)^3$ and $\delta V \propto R^3 \propto (1+z)^{-3\beta}$. Thus,

$$N_e \propto (1+z)^3 (1+z)^{-3\beta} (f(z)(1+z)^{\beta\gamma}). \tag{12}$$

The first two terms arise from the change in volume sampled. The final term, which may be seen by substituting $R(z)$ for $r$ in equation 10, expresses the change in physical scale sampled for the same comoving scale as a function of redshift. Assuming the number of galaxies physically in the cluster is a constant, $N_e$ is a constant, and re-arranging, gives $f(z) \propto (1+z)^{\beta(3-\gamma)-3}$. Equation 10 is therefore re-written as

$$\xi_{qg}(r,z) = B_{0,qg}(1+z)^{\nu} r^{-\gamma}; \qquad \nu = \beta(3-\gamma) - 3. \tag{13}$$

We substitute this form of the clustering evolution in place of that used by LS79, thus slightly modifying their equation expressing $w(\theta)$ in terms of spatial parameters. The final expression relating angular and spatial amplitudes is then

$$\frac{A_{qg}}{B_{0,qg}} = \frac{I_\gamma}{N_g} D^{3-\gamma} (1+z)^{\nu+\gamma} \varphi(m_0, z). \tag{14}$$

The only difference between this and the LS79 equation is the power to which the redshift dependent term is raised. $I_\gamma$ is a constant dependent only on the choice of slope for the

**Table 1.** Assumed galaxy morphology mix used in derivation of mean galaxy colours and K-corrections.

| Galaxy class | Fractional abundance |
|---|---|
| E / S0 | 0·35 |
| Sab | 0·20 |
| Sbc | 0·20 |
| Scd | 0·15 |
| Im | 0·10 |

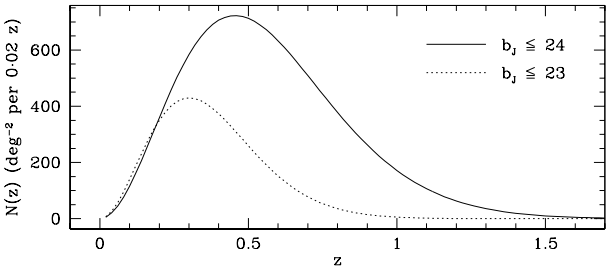


**Figure 3.** The galaxy redshift distributions adopted for the de-projection of the observed angular cross-correlation. They were derived from the functional form given by Efstathiou (1995). These may be compared with the QSO redshift distribution shown in Fig. 1.

power law in equation 10 and $D$ is the coordinate distance to the QSO.

$$D = \frac{cz}{H_0(1+z)}\left[\frac{1+z+\sqrt{1+2q_0z}}{1+q_0z+\sqrt{1+2q_0z}}\right] \quad (15)$$

$\varphi(m_0, z)$ is an integral luminosity function, i.e., the number of galaxies per comoving cubic mega-parsec with apparent magnitude brighter than the flux limit of the sample, $m_0$, at redshift, $z$. As described above, $\varphi$ may be expressed as $\mathrm{d}N/\mathrm{d}V$, the ratio of an observed $\mathrm{d}N/\mathrm{d}z$ and $\mathrm{d}V/\mathrm{d}z$, which is precisely specified by the chosen cosmology.

The value of $\beta$ then specifies the type of clustering evolution which is present. If $\beta = 1$, $\nu = -\gamma$ and the redshift dependence disappears giving comoving evolution. If $\beta = 0$, then $\nu = -3$ and the redshift term becomes $(1+z)^{-3+\gamma}$, which is the case for stable clustering as in LS79. This evolution has also been parameterised in the literature in terms of the equivalent term $\epsilon$, where $\epsilon = \beta(\gamma-3)$ and $\nu = -(3+\epsilon)$ (e.g., Efstathiou et al. 1991).

### 3.2 Practical estimators for $w_{qg}(\theta)$ and $A_{qg}$

For a single field, the QSO–galaxy cross-correlation may be estimated by

$$w_{qg}(\theta) = \frac{QG}{QR} - 1, \quad (16)$$

where $QG$ is the number of galaxies found in the range of separations $(\theta - \Delta\theta/2, \theta + \Delta\theta/2]$ from the QSO. $QR$ is the number of randomly scattered points in the same annulus. Random points were generated within the survey boundaries taking full account of any holes or complicated survey geometry. In order to minimise random errors, many times as many random 'galaxies' were generated as there are real galaxies in the field, and the counts scaled appropriately.

The clustering signal from any single QSO is very weak and has large associated uncertainties due to both Poisson errors and the intrinsic clustering of faint galaxies unrelated to the QSO. For most of the results presented here, the counts were coadded for all the fields within a given subsample (e.g., redshift slice), amounting to the pair-weighted average of $j$ fields calculated individually, i.e.,

$$w_{qg}(\theta) = \frac{\sum_{i=1}^{j} QG_i}{\sum_{i=1}^{j} QR_i} - 1. \quad (17)$$

The angular covariance amplitude was determined in two ways. If the full correlation function is plotted for a range of angular scales (e.g., Fig. 4), the best fitting value was found for the assumed form (equation 4) of the corelation function. Alternatively, if counts are taken in a single broad annulus around the QSO, the assumed form may be integrated to give a scaling factor from the mean correlation in the annulus (the observed quantity) to the amplitude at any chosen scale. This is the approach adopted where $A_{qg}$ must be determined from a single QSO field, e.g., Fig. 7. If $QG$ and $QR$ are the galaxy and random counts in the range $(\theta_{\min}, \theta_{\max}]$, then integrating equation 1 gives the excess counts above the background

$$QG - QR = \int_{\theta_{\min}}^{\theta_{\max}} 2\pi\theta N_g w_{qg}(\theta)\mathrm{d}\theta \quad (18a)$$

$$= \frac{2\pi\theta N_g A_{qg}}{3-\gamma}\left[\theta^{3-\gamma}\right]_{\theta_{\min}}^{\theta_{\max}}, \quad (18b)$$

using our standard assumed functional form for $w_{qg}(\theta)$. The background count, $QR$, is $\pi N_g(\theta_{\max}^2 - \theta_{\min}^2)$, which substituted into the above equation gives,

$$A_{qg} = \frac{3-\gamma}{2}\left(\frac{QG}{QR} - 1\right)\left(\frac{\theta_{\max}^2 - \theta_{\min}^2}{\theta_{\max}^{3-\gamma} - \theta_{\min}^{3-\gamma}}\right). \quad (19)$$

If the angles are normalised such that $\theta_{\max} = 1$, this formula gives the amplitude at the outer rim of the annulus. If they are expressed in degrees, it would be the amplitude at one degree and so forth.

### 3.3 Effects of poor star–galaxy separation

The correlation function thus far defined is the *true* correlation function, $w_t(\theta)$. In practice the galaxy catalogue is likely to be contaminated by stars or incomplete through the mis-classification of galaxies. Since the background count is taken from the total number of galaxies in the field, both $QG$ and $QR$ are biased, which in turn biases the *observed* correlation function, $w_o(\theta)$.

In the case of stellar contamination leading to an overestimate of the counts, it can straightforwardly be shown (e.g., Smith 1998) that:

$$w_t(\theta) = w_o(\theta)\left(1 + \frac{\mathcal{N}_S}{\mathcal{N}_G}\right). \quad (20)$$

$\mathcal{N}_G$ and $\mathcal{N}_S$ are the total numbers of galaxies and stars respectively found in the field. Since this is a multiplicative factor, the power-law shape remains unchanged. Neglecting to perform any star–galaxy separation, can therefore be corrected by rescaling the observed amplitude to its true value so long as the fractional contamination by stars is known.

The alternative case is accidental exclusion of galaxies from the catalogue. Assuming any such failure is random, both $QG$ and $QR$ counts have the same fractional error and the observed correlation function remains unchanged. Fewer counts do of course imply a lower statistical significance on any measurement. We note that the random errors assumption may not be entirely precise. Failures of the star–galaxy separation are unlikely to be entirely uncorrelated, perhaps having greater effect on galaxies in particular environments, magnitude ranges or regions of the image. We have been unable to detect any such systematic errors in the current data.

### 3.4 The Integral constraint, $I_B$

The true background number density of galaxies is not known precisely, so was estimated from the data. The background density was initially taken as the mean density within the particular field in question. If we then show that there is indeed a statistical excess of galaxies in the field, the estimated background value must have been biased high. The error may be retrospectively calculated from the observed correlation and the process iterated to self-consistent values. The fractional error in the background, $I_B$, or integral constraint, causes the true background to be overestimated by a factor $1+I_B$. $I_B$ is determined by integrating the correlation function over the full area of the field used.

$$I_B = \frac{\text{Integrated excess counts}}{\text{True background}} = \frac{\displaystyle\int_{\theta_{\min}}^{\theta_{\max}} 2\pi\theta w(\theta)\mathrm{d}\theta}{\displaystyle\int_{\theta_{\min}}^{\theta_{\max}} 2\pi\theta\mathrm{d}\theta} \quad (21)$$

assuming counts were taken from a circular region. For more complicated survey geometries, including holes in coverage, the quantity $I_B$ is more easily obtained by numerical integration over each field individually.

### 3.5 Errors on $w(\theta)$

Estimation of the errors on a correlation function and quantities determined therefrom is a subject of active debate (e.g., Landy & Szalay 1993, Mo, Jing & Börner 1992 and references therein). The measured amplitude of the auto-correlation function at any given scale is dependent on the distribution of the galaxies over a wide range of separations. Any individual galaxy will exist as one member of many different pairs, so the pair counts in any one counting annulus are not independent of counts in the neighbouring annuli. As a result, despite essentially being a counting statistic, the error on the pair counts is not in general Poissonian. The important distinction which must be drawn here is between an auto-correlation or full cross-correlation of two catalogues and the simplified geometry we are currently considering. This work simply azimuthally averages the number density of galaxies as a function of the radial distance from the QSO position. As a result, the galaxies in all pairs are independent so long as the fields do not overlap and the galaxy distribution is fully defined by the QSO–galaxy cross-correlation. In reality galaxies are clustered, so an assumption that galaxies' positions are independent is not true. It is however a very good approximation since any galaxy–galaxy clustering is washed out around the counting annulus. The error on the galaxy counts should then be very close to the $\sqrt{N}$ Poisson error. This was confirmed by a full bootstrap analysis (Barrow, Bhavsar & Sonoda 1984) of the errors (see Smith 1998) and so the Poisson error was adopted for this analysis.

## 4 RESULTS

### 4.1 Full data set, $0{\cdot}3 < z < 0{\cdot}7$

The cross-correlation, $w_{qg}(\theta)$, for all the QSOs with $V \leq 23$ galaxies is shown in Fig. 4. There is a positive correlation, though detected at a moderately weak level. At sub-arcminute separations there is a $2\sigma$ excess of galaxies over that expected for a random distribution and for the smallest counting annulus, approximately 22 arcsec, it is greater than $3\sigma$.

The $V \leq 23$ cut was chosen to correspond to about one magnitude fainter than the characteristic absolute magnitude, $M_V^* - 5\log h$, at $z \sim 0{\cdot}4$. It equals $M_V^* - 5\log h$ at $z \sim 0{\cdot}55$. This ensures that the peak of the galaxy $N(z)$ relation lies in the same redshift range as the QSOs. $M_V^*$, as a function of redshift, was taken from the $b_J < 24$ derived luminosity function of Ellis et al. (1996). Galaxy K-corrections (Oke & Sandage 1968) were taken from Pence (1976). Values for different galaxy types were averaged according to the Table 1 morphology mix and a linear fit made over the range $0{\cdot}3 < z < 0{\cdot}7$.

The predicted correlation functions for six different clustering amplitudes and evolution models have also been plotted in Fig. 4. Dashed lines are used for models stable in proper coordinates ($\beta = 0$, equation 13) and solid lines used

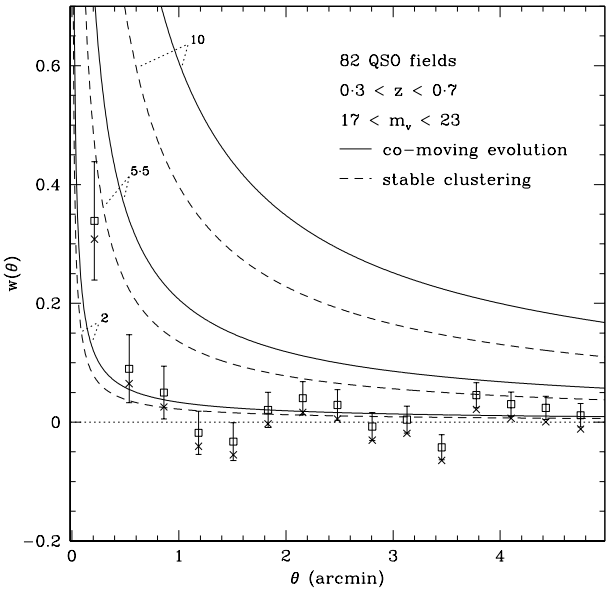


**Figure 4.** The cross-correlation function for all 82 $0{\cdot}3 < z < 0{\cdot}7$ QSOs with $V \leq 23$ galaxies. Crosses are the observed values. Open squares are modified by the integral constraint ($I_B = 11{\cdot}1A_{qg}$). The six curves show the expected signal for correlation lengths of $r_0 = 10$, $5{\cdot}5$ and $2\,h^{-1}$Mpc respectively from top to bottom. The solid and dashed lines represent $r_0$ as a constant in comoving and proper coordinates.

where $r_0$ is assumed to be stable in comoving coordinates ($\beta = 1$). To derive these curves, the correlation expected around each individual QSO was calculated (equation 14) assuming a power-law slope of $\gamma = 1{\cdot}8$ and the mean of the 82 separate amplitudes (one for each QSO field) is plotted. In this way, projection effects due to the redshift distribution of the QSOs are accounted for. Whereas equation 14 is integrated over the generalised, mean galaxy $N(z)$, this procedure effectively integrates over the $N(z)$ of the particular QSOs in the sample. The correlation lengths shown in Fig. 4 are 10, $5{\cdot}5$ and $2\,h^{-1}$Mpc, chosen to represent the following cases:

$r_0 = 2\,h^{-1}$Mpc: This is the correlation length of faint ($B > 22$) galaxies (e.g., Roche et al. 1993, Efstathiou 1995, Hudon & Lilly 1996).

$r_0 = 5{\cdot}5\,h^{-1}$Mpc: This is the present-day QSO–galaxy correlation length (Paper I). Also the galaxy correlation length, derived from bright, low-redshift galaxies has been measured by a variety of authors (e.g., Seldner & Peebles 1978, Davis & Peebles 1983) to be in the range $3{\cdot}4$ to $5{\cdot}5\,h^{-1}$Mpc (Koo & Szalay 1984).

$r_0 = 10\,h^{-1}$Mpc: This is an approximation to the clustering of galaxies around radio-loud QSOs. Yee & Green (1987) found correlation lengths of $8{\cdot}7$ and $17{\cdot}5\,h^{-1}$Mpc for radio-loud QSOs in the ranges $0{\cdot}3 < z < 0{\cdot}5$ and $0{\cdot}55 < z < 0{\cdot}65$ respectively. Using an enlarged data set, Ellingson et al. (1991) again found $r_0 \geq 15\,h^{-1}$Mpc for $0{\cdot}3 < z < 0{\cdot}6$, so $10\,h^{-1}$Mpc may be viewed as a lower limit.

For comparison, Loan, Wall & Lahav (1997) measured $r_0 \approx 18\,h^{-1}$Mpc for a mixed sample of radio galaxies

and radio-loud QSOs. Results from the FIRST radio survey are giving the lower value of 8–12 $h^{-1}$Mpc (Cress & Kamionkowsky 1998, Magliocchetti et al. 1998), possibly because the fainter flux limit is including many more starburst objects than the Parkes and Greenbank surveys used in the Loan et al. paper. Dalton et al. (1994) measured $r_0 \approx 14\,h^{-1}$Mpc for the galaxy cluster–cluster correlation length, but if we imagine that all QSOs are found in galaxy clusters, a more appropriate comparison might be with the cluster–galaxy cross-correlation, measured by Lilje & Efstathiou (1988) to be $r_0 = 8{\cdot}8\,h^{-1}$Mpc with $\gamma = 2{\cdot}2$.

From previous studies, a general picture has emerged of $B_{gg}$ being broadly similar to $B_{qg}$ for radio-quiet QSOs. Ellingson et al. (1991) measured a QSO–galaxy correlation length of $5{\cdot}6 \pm 3{\cdot}2\,h^{-1}$Mpc for their radio-quiet sample with no detectable variation over the range $0{\cdot}3 \leq z \leq 0{\cdot}6$. Boyle & Couch (1993) detected no significant clustering around their optically selected QSOs ($0{\cdot}9 \leq z \leq 1{\cdot}5$). Though their result ($r_0 = 0{\cdot}9 \pm 4{\cdot}0\,h^{-1}$Mpc) is consistent with a range of amplitudes up to and including the present-epoch galaxy covariance, it is inconsistent with the very rich environments measured by Tyson (1986) for radio-loud QSOs in the same redshift range. Croom & Shanks (1998) actually found a weak anti-correlation between $b_J < 23$ galaxies and optically selected QSOs. They show that this can be explained as an artifact caused by gravitational lensing, a conclusion consistent with the earlier study of Benítez & Martínez-González (1997) which used an even brighter magnitude limit of $b_J < 20{\cdot}5$.

In contrast, the results presented here are not consistent with the canonical $r_0 = 5{\cdot}5\,h^{-1}$Mpc galaxy correlations. Also, they are greatly inconsistent with correlations as strong as have been claimed for radio-loud QSOs or the galaxy–cluster cross-correlation. We know, however that faint galaxies are not found in the same average environments as bright galaxies either. Combining the results from five separate determinations of $A_{gg}$, Efstathiou (1995) found a constant comoving correlation length $r_0 = 2\,h^{-1}$Mpc to be a good fit for faint ($22 < b_J < 25{\cdot}5$) galaxies. A direct measurement of spatial clustering at moderate redshift from the *Canada-France Redshift Survey* (CFRS; Le Fèvre et al. 1996) also gave the same value of $r_0 = 2{\cdot}0\,h^{-1}$Mpc, assuming no evolution in comoving space between now and the mean redshift of the observations ($z = 0{\cdot}53$). These clustering amplitudes are consistent with the observations presented herein. As discussed by Le Fèvre et al. (1996), the inconsistency between observations at low and intermediate redshifts can be resolved either by assuming that a different population of galaxies is being probed by faint surveys, or conversely if the one population has undergone very significant evolution over the range $0 < z < 1$. The Le Fèvre et al. measurement of $r(z = 0{\cdot}53) = 1{\cdot}33 \pm 0{\cdot}09\,h^{-1}$Mpc is consistent with $r_0 = 5\,h^{-1}$Mpc if the evolution parameter, $\beta = -1{\cdot}6$. This is a very rapid evolution. A value of $\beta = -0{\cdot}667$ is predicted from $\Omega_0 = 1$ linear theory (Peebles 1988).

These results imply that radio-quiet QSOs apparently reside in environments consistent with those of the 'normal' galaxy population local to the QSO. We note however, that the observations are only $2\sigma$ inconsistent with there being no correlation at all, i.e., $r_0 = 0$, and our detection of clustering is not as secure as that in large galaxy redshift surveys such as the CFRS. Any 2D clustering results are equally consistent with an arbitrarily large correlation if we are prepared to accept the associated rapid evolution.

**Table 2.** Covariance amplitudes and the corresponding correlation lengths for $0{\cdot}3 < z < 0{\cdot}7$ QSOs and $V \leq 23$ galaxies under various assumed models of the clustering evolution, calculated from counts to one arcminute (equation 19).

| Covariance Amplitude $A$ (at 1 arcmin) | Correlation length $r_0$ ($h^{-1}$Mpc) | Inconsistency with 1 arcmin counts $\sigma$ |
|---|---|---|
| Observed | Derived | |
| $0{\cdot}054 \pm 0{\cdot}020$ | $2{\cdot}6 \pm 0{\cdot}6$ ($\beta = 1$) | – |
| $0{\cdot}054 \pm 0{\cdot}020$ | $3{\cdot}3 \pm 0{\cdot}6$ ($\beta = 0$) | – |
| Derived | Assumed | |
| $0{\cdot}606$ ($\beta = 1$) | 10 | 16 |
| $0{\cdot}398$ ($\beta = 0$) | 10 | 10 |
| $0{\cdot}207$ ($\beta = 1$) | 5·5 | 5·0 |
| $0{\cdot}135$ ($\beta = 0$) | 5·5 | 2·7 |
| $0{\cdot}033$ ($\beta = 1$) | 2·0 | 0·7 |
| $0{\cdot}022$ ($\beta = 0$) | 2·0 | 1·1 |
| 0·000 | 0 | 1·8 |

The covariance amplitudes for $0{\cdot}3 < z < 0{\cdot}7$ QSOs and $V \leq 23$ galaxies are summarised in Table 2. (The actual observed counts may be found in Table 3.) In the first two rows, the observed amplitude is determined from counts at less than 1 arcmin and converted to the correlation length, $r_0$. For the rest of table, assumed spatial-clustering models are converted to $A_{qg}$ via equation 14 for comparison. The final column gives the Poisson deviation required on the 1 arcmin galaxy counts to produce the suggested covariance amplitude. The most probable correlation lengths for non or slowly evolving clustering are around $3\,h^{-1}$Mpc. Correlation lengths as great as $r_0 = 5\,h^{-1}$Mpc become acceptable only if there is very rapid evolution in the clustering amplitude. Clustering comparable to that reported for radio-loud QSOs is strongly ruled out.

### 4.2 Subdivided data-sets

In order to investigate the parameters in the evolution model and to reduce the effect of clustering dilution along the line of sight, we sub-divided the sample in redshift. We also repeated the analysis for two sub-samples defined by absolute magnitude.

Observed 1 arcmin pair counts for the low ($0{\cdot}3 < z < 0{\cdot}5$) and high-redshift ($0{\cdot}5 < z < 0{\cdot}7$) samples are given in Table 3 and the cross-correlation functions are plotted in Fig. 5. Results from these samples demonstrate that most of the clustering seen in the full sample comes from the low-redshift fields, but that both sub-samples are consistent with either comoving or stable clustering with an $r_0$ of 2–3 $h^{-1}$Mpc. The $z < 0{\cdot}5$ data are best fit by $r_0 = 3{\cdot}6\,h^{-1}$Mpc, for virialized, stable clustering and $r_0 = 2{\cdot}9\,h^{-1}$Mpc for comoving clustering, assuming a $\gamma = 1{\cdot}8$ and the $A_{qg} = 0{\cdot}0028$ least-squares determination of the amplitude. The slightly weaker $A_{qg} = 0{\cdot}0026$ calculated from the one arcminute counts would give correlation lengths shorter than those quoted above by $0{\cdot}1\,h^{-1}$Mpc. The galaxy magnitude limits again correspond to $M^* - 5\log h + 1$ at the median redshift of the sub-sample. Inspection of Fig. 3 shows that in both cases

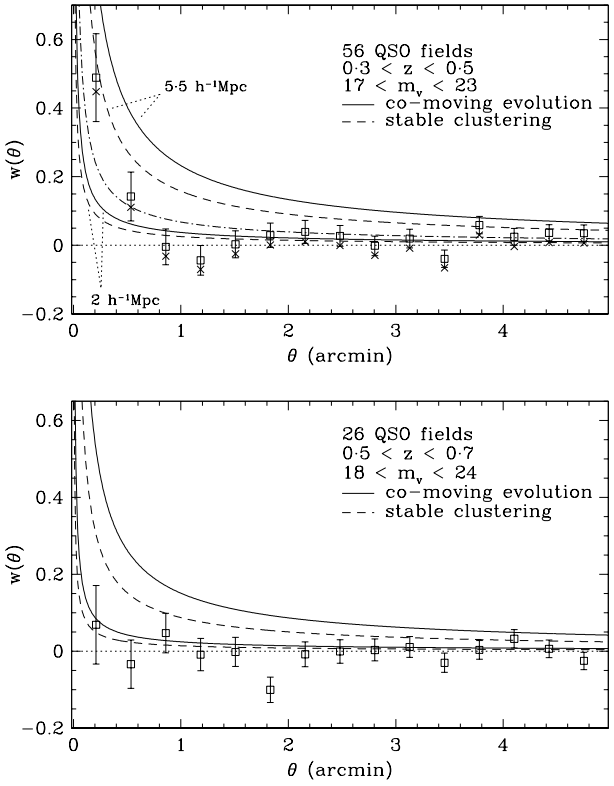


**Figure 5.** Cross correlations for $z < 0{\cdot}5$ and $z > 0{\cdot}5$ data plotted separately. In the upper, low-redshift panel, crosses are the raw, observed correlation and open squares are corrected for the integral constraint ($11{\cdot}0A_{qg}$). No correlation is detected in the higher-redshift sample, so no integral constraint is applicable. The dot-dashed curve in the upper panel is the measured amplitude of $A_{qg} = 0{\cdot}0026 \pm 0{\cdot}001$, which gives $r_0 = 2{\cdot}8\,h^{-1}$Mpc ($\beta = 1$). A least-squares best fit to the observations gave the consistent value, $A_{qg} = 0{\cdot}0028$. Comparison curves are for 5·5 and $2\,h^{-1}$Mpc as in Fig. 4.

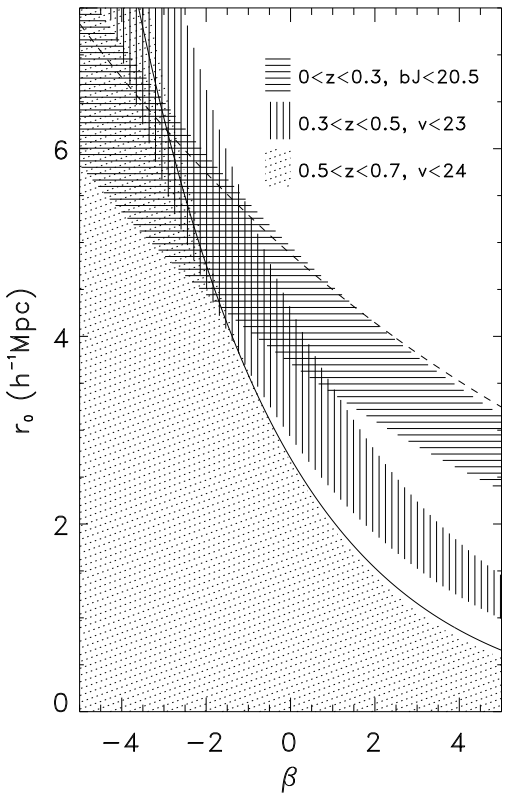


**Figure 6.** Values of $r_0, \beta$ which would be consistent with the present and previous observations. Shaded regions show $1\sigma$ limits on our observations of $A_{qg}$. The solid line represents $\xi_{gg}$ from the CFRS sample and the dashed line $w(\theta)_{gg}$ from the APM Galaxy Survey.

**Table 3.** Galaxy and random point raw counts at less than one arcminute from the QSO. $\sigma$ is the Poisson significance of $QG$'s difference from $QR$. Note that in two cases this is is a very small deficit rather than an excess, formally signifying an anti-correlation. After inclusion of the correction for 'detection success ratio' described in Section 2.5, these become a small, but insignificant positive correlation.

| QSO sub-sample | Galaxy magnitudes | $QG$ | $QR$ | $\sigma$ |
|---|---|---|---|---|
| $0{\cdot}3 < z < 0{\cdot}7$ | $17 < V < 23$ | 1008 | 948 | 1·9 |
| $0{\cdot}3 < z < 0{\cdot}5$ | $17 < V < 23$ | 691 | 640 | 1·9 |
| $0{\cdot}5 < z < 0{\cdot}7$ | $17 < V < 24$ | 725 | 729 | 0·15 |
| $M_V > -22$ | $17 < V < 23$ | 607 | 548 | 2·4 |
| $M_V < -22$ | $17 < V < 23$ | 401 | 403 | 0·08 |

the $N(z)$ distributions peak within an appropriate redshift range.

We can also combine the correlation length derived for the galaxy environments of $z < 0{\cdot}3$ QSOs in Paper I with those derived here to give us a large baseline over which to study the evolution of the clustering. A single measurement of the correlation defines a curve in the $r_0, \beta$ plane giving all possible value pairs consistent with the observation. Fig. 6 shows the regions of this plane bounded by the $1\sigma$ uncertainties on our clustering amplitude determinations, $0 < z < 0{\cdot}3$, $0{\cdot}3 < z < 0{\cdot}5$ and $0{\cdot}5 < z < 0{\cdot}7$. The high-redshift sample only defines an upper limit. Also plotted are two curves taken as examples of $\xi_{gg}$ measurements. The dashed line is for $b_J < 20$ galaxies from the APM Galaxy Survey (Baugh 1996) which have a median redshift, $z_m = 0{\cdot}13$. The solid line is for the CFRS ($I < 22{\cdot}5$), which has median redshift, $z_m = 0{\cdot}53$. These are not necessarily absolutely comparable to our amplitudes, since although they cover very similar redshift ranges, they have different magnitude limits and used slightly flatter power-laws to fit the clustering amplitude. They are however in reasonably good agreement.

The various observations may thus be reconciled if there has been moderately strong evolution in the clustering amplitude, $\beta < -1$ for both $\xi_{qg}$ and $\xi_{gg}$. Such a conclusion must assume that the same single population is being sampled in each experiment.

Alternatively, rather than summing the data over a predefined redshift range, in Fig. 7 the observed amplitude at one arcminute is plotted as a function of redshift for each QSO individually. The top panel shows the amplitude for each of the 82 fields with their individual error bars and three constant comoving correlation length models. In the

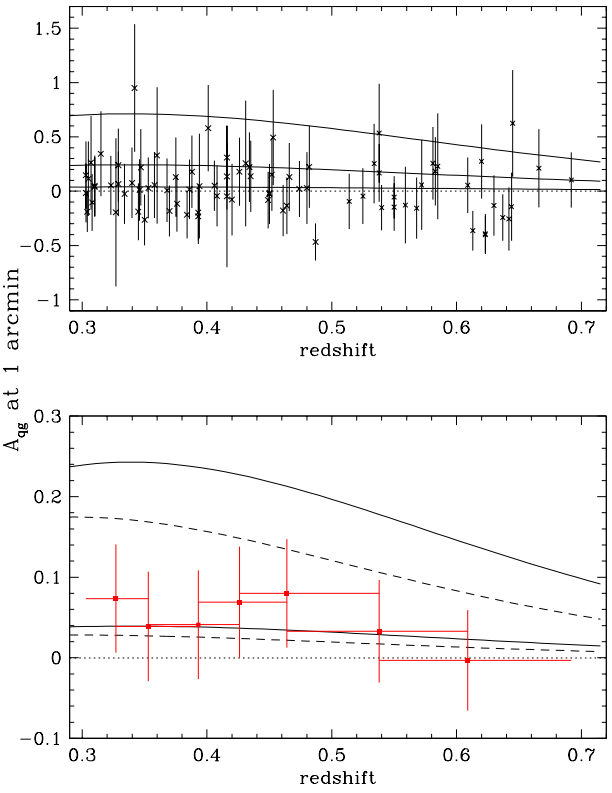


**Figure 7.** Observed QSO–galaxy cross-correlation amplitude at one arcminute using $V \leq 23$ galaxies. The two panels show the same data with an axis re-scaled for clarity. In the top panel, curves representing 10, 5·5 and $2\,h^{-1}$Mpc comoving correlation functions are shown. In the lower panel, only 5·5 and $2\,h^{-1}$Mpc are visible. Solid curves are for constant comoving evolution and dashed for constant proper correlation length. Filled boxes are each the average of eleven fields and the error bars give the one sigma standard deviation in each subsample.

lower panel, the $A_{qg}$ axis is re-scaled for clarity. Filled boxes are each the average of eleven fields, thereby adaptively sampling the redshift range according to the availability of data. The $r_0 = 5{\cdot}5\,h^{-1}$Mpc and $2\,h^{-1}$Mpc, comoving and stable clustering models are also plotted in the lower panel. This demonstrates that the summed data in the redshift slices are representative and are not strongly dependent on any single, or few, fields. There are significantly more positive points than negative in the $z < 0{\cdot}5$, $V \leq 23$ data. When a similar plot is produced with a limiting galaxy magnitude $V \leq 24$, which we consider more appropriate for $0{\cdot}5 < z < 0{\cdot}7$ QSOs, the data points are almost exactly evenly split around the $A_{qg} = 0$ axis at all redshifts, giving agreement with the zero correlation seen in the lower panel of Fig. 5.

The plot also shows that the predicted change in amplitude over the redshift range studied is small and the curves for different values of the parameter $\beta$ are similar in shape. An order of magnitude increase in the number of QSO fields observed would be required to reliably distinguish between these two clustering evolution schemes.

Finally, the clustering amplitude as a function of QSO absolute magnitude is shown in Fig. 8. Amplitudes are here plotted in terms of the spatial covariance to compensate for the different projection effects on QSOs of the same absolute magnitude, but different redshifts. The amplitude appears to decrease with increasing QSO luminosity. This is markedly different to the rapid increase in cluster richness with QSO luminosity seen by Yee & Green (1987) for radio-loud QSOs. Caution must be exercised when assigning any significance to the apparent variation seen in Fig. 8. Figs 7 and 8 are not independent since luminosity and redshift are related via the QSO luminosity evolution. Indeed, from Fig. 1 it is clear that 80 per cent of the $M_V - 5\log h > -22$ QSOs are also in the $z < 0{\cdot}5$ sub-sample. What appears to be a correlation with luminosity may simply be the selection function being influenced by the evolving QSO luminosity function. Allowing for this, there is no evidence in the current data for a dependence on luminosity which is independent from that with redshift.

### 4.3 Comparison with QSO and galaxy autocorrelations

In the previous section we showed that, at intermediate redshifts, $0{\cdot}3 < z < 0{\cdot}7$, the inferred clustering scale length for faint galaxies around QSOs, $r_0 = 2\,h^{-1}$Mpc was similar to that derived from the auto-correlation function of faint galaxies, and thus, in the simplest interpretation, the QSOs and faint galaxies might exhibit the same bias. In contrast, the most recent measurements of the QSO correlation function are consistent with a constant comoving amplitude $r_0 = 5\,h^{-1}$Mpc at $z \leq 2{\cdot}2$ (Croom & Shanks 1996), suggesting QSOs are strongly biased with respect to the galaxy population if the galaxy scale length is $r_0 = 2\,h^{-1}$Mpc. However, the measurement of the QSO correlation length is dominated by QSOs with $1 < z < 2$, with relatively few QSOs at $0{\cdot}3 < z < 0{\cdot}7$ and certainly too few to rule out $r_0 = 2\,h^{-1}$Mpc for the QSO correlation length at these redshifts.

If the galaxy correlation length were to increase again at $z > 1$ then the QSO and galaxy distribution could be reconciled with the same value for the bias parameter (albeit redshift dependent). There is some evidence that the galaxy correlation must increase again at higher redshift; angular correlations for HDF galaxies with photometric redshifts shown a rapid increase at $z \sim 2$ (Magliocchetti & Maddox 1999, Arnouts et al 1999), and Giavalisco et al. (1998) measure $r_0 = 6\,h^{-1}$Mpc for galaxies at $z \sim 3$. Alternatively, the strong clustering seen for both QSOs and the Giavalisco et al. galaxies may simply be highlighting the danger of generalising from any one type of galaxy to another when we do not understand galaxy formation and how the classes are inter-related. Such discrepancies are seen also for 'normal' galaxies, even within a single, optically selected survey. For example, both the luminosity functions (Lilly et al. 1995) and correlation functions (Le Fèvre et al. 1996) of red and blue galaxies in the CFRS show significantly different evolution over the redshift range $0 < z < 0{\cdot}8$ and in comparison to the present epoch determinations.

### 4.4 Future work

It is clear that we do not yet understand the cluster environments of QSOs with the same precision as we do for galaxies. New wide-field CCD cameras on large-aperture telescopes

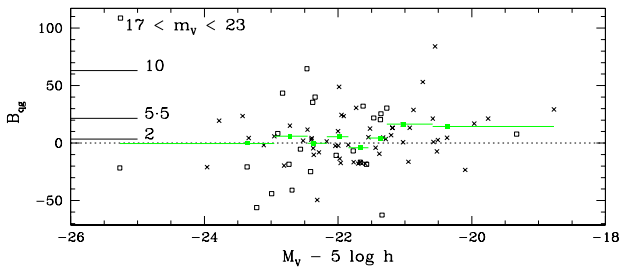


**Figure 8.** QSO–galaxy spatial covariance amplitude, assuming $\beta = 1$, as a function of QSO absolute magnitude. Crosses are $z < 0{\cdot}5$, open boxes $z > 0{\cdot}5$. Horizontal bars on the left of the plot indicate the amplitudes equivalent to correlation lengths, $r_0 = 2$, $5{\cdot}5$ and $10\,h^{-1}$Mpc. $M_V > -22$ is almost a subset of $z < 0{\cdot}5$, so trends in $B_{qg}$ from this plot and Fig. 7 are not independent.

will be able to make some contribution to these studies, but the broad range in redshift of galaxies in a simply flux-limited sample places a significant limit on the sensitivity of this approach. The ever improving availability of redshift data for faint galaxies will go some way to allowing detailed studies of QSO environments, though even the upcoming generation of sky surveys will not probe to sufficiently faint limits to obtain redshifts for typical $M^*$ galaxies at the redshifts investigated here. Photometric redshifts obtained from wide-field imaging in several pass-bands may prove the most efficient method to further the work described here. The potential for photometric redshifts at $z < 2$ has been proved through recent interest in the technique spurred by the Hubble Deep Field (e.g., Fernández-Soto, Lanzetta & Yahil 1998).

## 5 SUMMARY

Clustering of $V < 23$ galaxies around X-ray-selected, $0{\cdot}3 < z < 0{\cdot}7$ QSOs has been detected with a $>2\sigma$ significance. The amplitude of the correlation function is small, $A_{qg}(1^\circ) = 0{\cdot}0020 \pm 0{\cdot}0008$, implying a spatial clustering of amplitude $r_0 \approx 3\,h^{-1}$Mpc. Though not a secure detection of clustering around X-ray selected QSOs, it is a highly significant rejection of rich cluster environments similar to those found for radio loud QSOs (Yee & Green 1987), and of the cluster environment around present day normal galaxies.

When the sample was subdivided at $z = 0{\cdot}5$, the correlation was found to be stronger in the $z < 0{\cdot}5$ data. No significant excess of QSO–galaxy pairs over the mean background counts was observed at $z > 0{\cdot}5$. The best-fitting amplitude for the low-redshift sample was $A_{qg}(1^\circ) = 0{\cdot}0026 \pm 0{\cdot}001$, which corresponds to $r_0 \approx 3\,h^{-1}$Mpc if we assume there has been little evolution in the clustering since $z = 0{\cdot}5$.

These measured correlation amplitudes are in good agreement with measurements of the faint-galaxy correlation function (e.g., Roche et al. 1993, Le Fèvre et al. 1996). Taken in conjunction with the results of Paper I, this implies that QSOs are likely to be populating average galaxy environments at all redshifts $z < 0{\cdot}5$. Though no clustering was detected for the $z > 0{\cdot}5$ subsample or in the high-redshift sample of Boyle & Couch (1993), these null results too are consistent with the same conclusion. This is in very marked contrast to the rapid evolution in the richness of galaxy clusters associated with radio-loud QSOs, which by $z \sim 0{\cdot}6$ are typically found in Abell richness class 1 clusters (Yee & Green 1984, Ellingson et al. 1991). While further work remains to be done, the results here indicate that radio-quiet QSOs may not be strongly biased with respect to the galaxy population. This has important, and potentially positive, consequences for studies of large-scale structure from the forthcoming large QSO redshift surveys.

## ACKNOWLEDGEMENTS

RJS acknowledges the financial support of the United Kingdom Particle Physics and Astronomy Research Council and would also like to thank the Anglo-Australian Observatory for their generous hospitality during a one-year visit to their Epping laboratory, where much of this work was conducted.

## REFERENCES

Arnouts S., Cristiani S., Moscardini L., Matarrese S., Lucchin F., Fontana A., Giallongo E., 1999, MNRAS, submitted, astro-ph/9902290
Avni Y., Tananbaum H., 1986, ApJ, 305, 83
Bahcall J.H., Soneira R.M., 1980, ApJS, 44, 73
Barrow J.D., Bhavsar S.P., Sonoda D.H., 1984 MNRAS, 210, 19
Baugh C.M., 1996, MNRAS, 280, 267
Baugh C.M., Efstathiou G., 1993, MNRAS, 265, 145
Benítez N., Martínez-González E., 1997, ApJ, 477, 27
Bertin E., Arnouts S., 1996, A&AS, 117, 393
Blair M., Gilmore G., 1982, PASP, 94, 742
Boyle B.J., Couch W.J., 1993, MNRAS, 264, 604
Boyle B.J., Di Matteo T., 1995, MNRAS, 277, L63
Boyle B.J., Mo H.J., 1993, MNRAS, 260, 925
Boyle B.J., Wilkes B.J., Elvis M., 1997, MNRAS, 285, 511
Boyle B.J, Croom S.M, Smith R.J, Shanks T., Miller L., 1998, in Ellis R.S. and Efstathiou G. eds *Large Scale Structure in the Universe*, Phil. Trans. Roy. Soc. B., in press
Chu Y., Zhao Y.-H., 1997, in McLean B.J., Golombek D.A., Hayes J.J.E., Payne E., eds, I.A.U. Symp. 179, *New Horizons from Multi-Wavelength Sky Surveys*, Kluwer, Dordrecht, p. 131
Cress C.M., Kamionkowsky M., 1998, astro-ph/9801284
Croom S.M., Shanks T., (1996), MNRAS, 281, 893
Croom S.M., Shanks T., (1998), MNRAS, submitted
Dalton G.B., Croft R.A.C., Efstathiou G., Sutherland W.J., Maddox S.J., Davis M., 1994, MNRAS, 271, 47P
Davis M., Peebles P.J.E., 1983, ApJ, 267, 465
Della Ceca R., Zamorani G., Maccacaro T., Wolter A., Griffiths R., Stocke J.T., Setti G., 1994, ApJ, 430, 533
Driver S.P., Phillipps S., Davies J.I., Morgan I., Disney M.J., 1994, MNRAS, 266, 155
Efstathiou G., Bernstein G., Katz N., Tyson J.A., Guhathakurta P., 1991, ApJL, 380, 47
Efstathiou G., 1995, MNRAS, 272, 25P
Ellingson E., Yee H.K.C., Green R.F., 1991, ApJ, 371, 49
Ellis R.S., Colless M., Broadhurst T., Heyl J., Glazebrook K., 1996, MNRAS, 280, 235
Fernández-Soto A., Lanzetta K.M., Yahil A., 1998, ApJ, 513, 34
Fukugita M., Shimasaku K., Ichikawa T., 1995, PASP, 107, 945
Giavalisco M., Steidel C.C., Adelberger K.L, Dickinson M.E., Pettini M., Kellogg M., ApJ, 1998, 503, 543
Glazebrook K., Ellis R., Colless M., Broadhurst T., Allington-Smith J., Tanvir N., 1995, MNRAS, 273, 157
Groth E.J., Peebles P.J.E., 1977, ApJ, 217, 385

Hudon J.D., Lilly S.J., 1996, ApJ, 469, 519
Koo D.C., Szalay A.S., 1984, ApJ, 282, 390
Landy S.D., Szalay A.S., 1993, ApJ, 412, 64
La Franca F., Andreani P., Cristiani S., 1998, ApJ, 497, 529
Le Fèvre O., Hudon D., Lilly S.J., Crampton D., 1996, ApJ, 461, 534
Lilje P.B., Efstathiou G., 1998, MNRAS, 231, 635
Lilly S.J., Tresse L., Hammer F., Crampton D., Le Fèvre O., 1995, ApJ, 455, 108
Limber D.N., 1953, ApJ, 117, 134
Loan A.J., Wall J.V., Lahav O., 1997, MNRAS, 286, 994
Longair M.S., Seldner M., 1979, MNRAS, 189, 433, **LS79**
Maddox S.J., Efstathiou G., Sutherland W.J., Loveday J., 1990a, MNRAS, 242, 43P
Maddox S.J., Efstathiou G., Sutherland W.J., 1996, MNRAS, 283, 1227
Magliocchetti M., Maddox S.J., Lahav O., Wall J.V., 1998, MNRAS, 300, 257
Magliocchetti M., Maddox S.J., 1999, MNRAS, 306, 988
Mo H.J., Jing Y.P., Börner G., 1992, ApJ, 392, 452
Oke J.B., Sandage A., 1968, 154, 210
Peebles P.J.E., 1988, The Large-Scale Structure of the Universe, Princeton Univ. Press, Princeton
Pence W., 1976, ApJ, 203, 39
Phillipps S., Fong R., Ellis R.S., Fall S.M., MacGillivray H.T., 1978, MNRAS, 182, 673
Prestage R.M., Peacock J.A., 1988, MNRAS, 230, 131
Roche N., Shanks T., Metcalfe N, Fong R., 1993, MNRAS, 263, 360
Seldner M., Peebles P.J.E., 1978, ApJ, 225, 7
Smail I., Ellis R.S., Fitchett M.J., 1994, MNRAS, 270, 245
Smail I., Hogg D.W., Yan L., Cohen J.G., 1995, ApJL, 449, 105
Smith R.J., Boyle B.J., Maddox S.J., 1995, MNRAS, 277, 270 **Paper I**
Smith R.J., 1998, PhD Thesis, University of Cambridge
Stocke J.T., Morris S.L., Gioia I.M., Maccacaro T., Schild R., Wolter A., Fleming T.A., Henry J.P., 1991, ApJS, 76, 813
Tyson J.A., 1986, AJ, 92, 691
Yates M.G., Miller L., Peacock J.A., 1989, MNRAS, 240, 129
Yee H.K.C., Green R.F., 1984, ApJ, 280, 79
Yee H.K.C., Green R.F., 1987, ApJ, 319, 28
Zamorani G. et al., 1981, ApJ, 245, 357

This paper has been produced using the Royal Astronomical Society/Blackwell Science TEX macros.